

# Search for Baryonic Resonances Decaying to $\Xi\pi$ in Deep-Inelastic Scattering at HERA

H1 Collaboration

## Abstract

A search for narrow baryonic resonances decaying into  $\Xi^-\pi^-$  or  $\Xi^-\pi^+$  and their antiparticles is carried out with the H1 detector using deep inelastic scattering events at HERA in the range of negative photon four-momentum transfer squared  $2 < Q^2 < 100 \text{ GeV}^2$ . No signal is observed for a new baryonic state in the mass range  $1600 - 2300 \text{ MeV}$  in either the doubly charged or the neutral decay channels. The known baryon  $\Xi(1530)^0$  is observed through its decay mode into  $\Xi^-\pi^+$ . Upper limits are given on the ratio of the production rates of new baryonic states, such as the hypothetical pentaquark states  $\Xi_{5q}^{--}$  or  $\Xi_{5q}^0$ , relative to the  $\Xi(1530)^0$  baryon state.

To be submitted to Phys. Lett. **B**

A. Aktas<sup>10</sup>, C. Alexa<sup>10,49</sup>, V. Andreev<sup>24</sup>, T. Anthonis<sup>4</sup>, B. Antunovic<sup>25</sup>, S. Aplin<sup>10</sup>,  
 A. Asmone<sup>32</sup>, A. Astvatsatourov<sup>4</sup>, S. Backovic<sup>29</sup>, A. Baghdasaryan<sup>37</sup>, P. Baranov<sup>24</sup>,  
 E. Barrelet<sup>28</sup>, W. Bartel<sup>10</sup>, S. Baudrand<sup>26</sup>, M. Beckingham<sup>10</sup>, K. Begzsuren<sup>34</sup>, O. Behnke<sup>13</sup>,  
 O. Behrendt<sup>7</sup>, A. Belousov<sup>24</sup>, N. Berger<sup>39</sup>, J.C. Bizot<sup>26</sup>, M.-O. Boenig<sup>7</sup>, V. Boudry<sup>27</sup>,  
 I. Bozovic-Jelisavcic<sup>2</sup>, J. Bracinik<sup>25</sup>, G. Brandt<sup>13</sup>, M. Brinkmann<sup>10</sup>, V. Brisson<sup>26</sup>,  
 D. Bruncko<sup>15</sup>, F.W. Büsser<sup>11</sup>, A. Bunyatyan<sup>12,37</sup>, G. Buschhorn<sup>25</sup>, L. Bystritskaya<sup>23</sup>,  
 A.J. Campbell<sup>10</sup>, K.B. Cantun Avila<sup>21</sup>, F. Cassol-Brunner<sup>20</sup>, K. Cerny<sup>31</sup>, V. Cerny<sup>15,46</sup>,  
 V. Chekelian<sup>25</sup>, A. Cholewa<sup>10</sup>, J.G. Contreras<sup>21</sup>, J.A. Coughlan<sup>5</sup>, G. Cozzika<sup>9</sup>, J. Cvach<sup>30</sup>,  
 J.B. Dainton<sup>17</sup>, K. Daum<sup>36,42</sup>, M. Deak<sup>10</sup>, Y. de Boer<sup>23</sup>, B. Delcourt<sup>26</sup>, M. Del Degan<sup>39</sup>,  
 A. De Roeck<sup>10,44</sup>, E.A. De Wolf<sup>4</sup>, C. Diaconu<sup>20</sup>, V. Dodonov<sup>12</sup>, A. Dubak<sup>29,45</sup>, G. Eckerlin<sup>10</sup>,  
 V. Efremenko<sup>23</sup>, S. Egli<sup>35</sup>, R. Eichler<sup>35</sup>, F. Eisele<sup>13</sup>, A. Eliseev<sup>24</sup>, E. Elsen<sup>10</sup>, S. Essenov<sup>23</sup>,  
 A. Falkewicz<sup>6</sup>, P.J.W. Faulkner<sup>3</sup>, L. Favart<sup>4</sup>, A. Fedotov<sup>23</sup>, R. Felst<sup>10</sup>, J. Feltesse<sup>9,47</sup>,  
 J. Ferencei<sup>15</sup>, L. Finke<sup>10</sup>, M. Fleischer<sup>10</sup>, A. Fomenko<sup>24</sup>, G. Franke<sup>10</sup>, T. Frisson<sup>27</sup>,  
 E. Gabathuler<sup>17</sup>, E. Garutti<sup>10</sup>, J. Gayler<sup>10</sup>, S. Ghazaryan<sup>37</sup>, S. Ginzburgskaya<sup>23</sup>, A. Glazov<sup>10</sup>,  
 I. Glushkov<sup>38</sup>, L. Goerlich<sup>6</sup>, M. Goettlich<sup>10</sup>, N. Gogitidze<sup>24</sup>, S. Gorbounov<sup>38</sup>, M. Gouzevitch<sup>27</sup>,  
 C. Grab<sup>39</sup>, T. Greenshaw<sup>17</sup>, B.R. Grell<sup>10</sup>, G. Grindhammer<sup>25</sup>, S. Habib<sup>11,48</sup>, D. Haidt<sup>10</sup>,  
 M. Hansson<sup>19</sup>, G. Heinzelmann<sup>11</sup>, C. Helebrant<sup>10</sup>, R.C.W. Henderson<sup>16</sup>, H. Henschel<sup>38</sup>,  
 G. Herrera<sup>22</sup>, M. Hildebrandt<sup>35</sup>, K.H. Hiller<sup>38</sup>, D. Hoffmann<sup>20</sup>, R. Horisberger<sup>35</sup>,  
 A. Hovhannisyan<sup>37</sup>, T. Hreus<sup>4,43</sup>, M. Jacquet<sup>26</sup>, M.E. Janssen<sup>10</sup>, X. Janssen<sup>4</sup>, V. Jemanov<sup>11</sup>,  
 L. Jönsson<sup>19</sup>, D.P. Johnson<sup>4</sup>, A.W. Jung<sup>14</sup>, H. Jung<sup>10</sup>, M. Kapichine<sup>8</sup>, J. Katzy<sup>10</sup>, I.R. Kenyon<sup>3</sup>,  
 C. Kiesling<sup>25</sup>, M. Klein<sup>17</sup>, C. Kleinwort<sup>10</sup>, T. Klimkovich<sup>10</sup>, T. Kluge<sup>10</sup>, A. Knutsson<sup>19</sup>,  
 V. Korbel<sup>10</sup>, P. Kostka<sup>38</sup>, M. Kraemer<sup>10</sup>, K. Krastev<sup>10</sup>, J. Kretzschmar<sup>38</sup>, A. Kropivnitskaya<sup>23</sup>,  
 K. Krüger<sup>14</sup>, M.P.J. Landon<sup>18</sup>, W. Lange<sup>38</sup>, G. Laštovička-Medin<sup>29</sup>, P. Laycock<sup>17</sup>,  
 A. Lebedev<sup>24</sup>, G. Leibenguth<sup>39</sup>, V. Lendermann<sup>14</sup>, S. Levonian<sup>10</sup>, L. Lindfeld<sup>40</sup>, K. Lipka<sup>11</sup>,  
 A. Liptaj<sup>25</sup>, B. List<sup>11</sup>, J. List<sup>10</sup>, N. Loktionova<sup>24</sup>, R. Lopez-Fernandez<sup>22</sup>, V. Lubimov<sup>23</sup>,  
 A.-I. Lucaci-Timoce<sup>10</sup>, L. Lytkin<sup>12</sup>, A. Makankine<sup>8</sup>, E. Malinovski<sup>24</sup>, P. Marage<sup>4</sup>, Ll. Marti<sup>10</sup>,  
 M. Martisikova<sup>10</sup>, H.-U. Martyn<sup>1</sup>, S.J. Maxfield<sup>17</sup>, A. Mehta<sup>17</sup>, K. Meier<sup>14</sup>, A.B. Meyer<sup>10</sup>,  
 H. Meyer<sup>10</sup>, H. Meyer<sup>36</sup>, J. Meyer<sup>10</sup>, V. Michels<sup>10</sup>, S. Mikocki<sup>6</sup>, I. Milcewicz-Mika<sup>6</sup>,  
 D. Mladenov<sup>33</sup>, A. Mohamed<sup>17</sup>, F. Moreau<sup>27</sup>, A. Morozov<sup>8</sup>, J.V. Morris<sup>5</sup>, M.U. Mozer<sup>13</sup>,  
 K. Müller<sup>40</sup>, P. Murín<sup>15,43</sup>, K. Nankov<sup>33</sup>, B. Naroska<sup>11</sup>, Th. Naumann<sup>38</sup>, P.R. Newman<sup>3</sup>,  
 C. Niebuhr<sup>10</sup>, A. Nikiforov<sup>25</sup>, G. Nowak<sup>6</sup>, K. Nowak<sup>40</sup>, M. Nozicka<sup>38</sup>, R. Oganezov<sup>37</sup>,  
 B. Olivier<sup>25</sup>, J.E. Olsson<sup>10</sup>, S. Osman<sup>19</sup>, D. Ozerov<sup>23</sup>, V. Palichik<sup>8</sup>, I. Panagoulas<sup>1,10,41</sup>,  
 M. Pandurovic<sup>2</sup>, Th. Papadopoulou<sup>1,10,41</sup>, C. Pascaud<sup>26</sup>, G.D. Patel<sup>17</sup>, H. Peng<sup>10</sup>, E. Perez<sup>9</sup>,  
 D. Perez-Astudillo<sup>21</sup>, A. Perieanu<sup>10</sup>, A. Petrukhin<sup>23</sup>, I. Picuric<sup>29</sup>, S. Piec<sup>38</sup>, D. Pitzl<sup>10</sup>,  
 R. Plačakytė<sup>10</sup>, B. Povh<sup>12</sup>, T. Preda<sup>10,49</sup>, P. Prideaux<sup>17</sup>, A.J. Rahmat<sup>17</sup>, N. Raicevic<sup>29</sup>,  
 T. Ravdandorj<sup>34</sup>, P. Reimer<sup>30</sup>, A. Rimmer<sup>17</sup>, C. Risler<sup>10</sup>, E. Rizvi<sup>18</sup>, P. Robmann<sup>40</sup>, B. Roland<sup>4</sup>,  
 R. Roosen<sup>4</sup>, A. Rostovtsev<sup>23</sup>, Z. Rurikova<sup>10</sup>, S. Rusakov<sup>24</sup>, F. Salvaire<sup>10</sup>, D.P.C. Sankey<sup>5</sup>,  
 M. Sauter<sup>39</sup>, E. Sauvan<sup>20</sup>, S. Schmidt<sup>10</sup>, S. Schmitt<sup>10</sup>, C. Schmitz<sup>40</sup>, L. Schoeffel<sup>9</sup>,  
 A. Schöning<sup>39</sup>, H.-C. Schultz-Coulon<sup>14</sup>, F. Sefkow<sup>10</sup>, R.N. Shaw-West<sup>3</sup>, I. Sheviakov<sup>24</sup>,  
 L.N. Shtarkov<sup>24</sup>, T. Sloan<sup>16</sup>, I. Smiljanic<sup>2</sup>, P. Smirnov<sup>24</sup>, Y. Soloviev<sup>24</sup>, D. South<sup>7</sup>, V. Spaskov<sup>8</sup>,  
 A. Specka<sup>27</sup>, Z. Staykova<sup>10</sup>, M. Steder<sup>10</sup>, B. Stella<sup>32</sup>, J. Stiewe<sup>14</sup>, U. Straumann<sup>40</sup>, D. Sunar<sup>4</sup>,  
 T. Sykora<sup>4</sup>, V. Tchoulakov<sup>8</sup>, G. Thompson<sup>18</sup>, P.D. Thompson<sup>3</sup>, T. Toll<sup>10</sup>, F. Tomasz<sup>15</sup>,  
 D. Traynor<sup>18</sup>, T.N. Trinh<sup>20</sup>, P. Truöl<sup>40</sup>, I. Tsakov<sup>33</sup>, B. Tseepeldorj<sup>34</sup>, G. Tsipolitis<sup>10,41</sup>,  
 I. Tsurin<sup>38</sup>, J. Turnau<sup>6</sup>, E. Tzamariudaki<sup>25</sup>, K. Urban<sup>14</sup>, D. Utkin<sup>23</sup>, A. Valkárová<sup>31</sup>, C. Vallée<sup>20</sup>,  
 P. Van Mechelen<sup>4</sup>, A. Vargas Trevino<sup>10</sup>, Y. Vazdik<sup>24</sup>, S. Vinokurova<sup>10</sup>, V. Volchinski<sup>37</sup>,  
 G. Weber<sup>11</sup>, R. Weber<sup>39</sup>, D. Wegener<sup>7</sup>, C. Werner<sup>13</sup>, M. Wessels<sup>10</sup>, Ch. Wissing<sup>10</sup>, R. Wolf<sup>13</sup>,

E. Wunsch<sup>10</sup>, S. Xella<sup>40</sup>, V. Yeganov<sup>37</sup>, J. Žáček<sup>31</sup>, J. Zálešák<sup>30</sup>, Z. Zhang<sup>26</sup>, A. Zhelezov<sup>23</sup>, A. Zhokin<sup>23</sup>, Y.C. Zhu<sup>10</sup>, T. Zimmermann<sup>39</sup>, H. Zohrabyan<sup>37</sup>, and F. Zomer<sup>26</sup>

- <sup>1</sup> *I. Physikalisches Institut der RWTH, Aachen, Germany<sup>a</sup>*
- <sup>2</sup> *Vinca Institute of Nuclear Sciences, Belgrade, Serbia*
- <sup>3</sup> *School of Physics and Astronomy, University of Birmingham, Birmingham, UK<sup>b</sup>*
- <sup>4</sup> *Inter-University Institute for High Energies ULB-VUB, Brussels; Universiteit Antwerpen, Antwerpen; Belgium<sup>c</sup>*
- <sup>5</sup> *Rutherford Appleton Laboratory, Chilton, Didcot, UK<sup>b</sup>*
- <sup>6</sup> *Institute for Nuclear Physics, Cracow, Poland<sup>d</sup>*
- <sup>7</sup> *Institut für Physik, Universität Dortmund, Dortmund, Germany<sup>a</sup>*
- <sup>8</sup> *Joint Institute for Nuclear Research, Dubna, Russia*
- <sup>9</sup> *CEA, DSM/DAPNIA, CE-Saclay, Gif-sur-Yvette, France*
- <sup>10</sup> *DESY, Hamburg, Germany*
- <sup>11</sup> *Institut für Experimentalphysik, Universität Hamburg, Hamburg, Germany<sup>a</sup>*
- <sup>12</sup> *Max-Planck-Institut für Kernphysik, Heidelberg, Germany*
- <sup>13</sup> *Physikalisches Institut, Universität Heidelberg, Heidelberg, Germany<sup>a</sup>*
- <sup>14</sup> *Kirchhoff-Institut für Physik, Universität Heidelberg, Heidelberg, Germany<sup>a</sup>*
- <sup>15</sup> *Institute of Experimental Physics, Slovak Academy of Sciences, Košice, Slovak Republic<sup>f</sup>*
- <sup>16</sup> *Department of Physics, University of Lancaster, Lancaster, UK<sup>b</sup>*
- <sup>17</sup> *Department of Physics, University of Liverpool, Liverpool, UK<sup>b</sup>*
- <sup>18</sup> *Queen Mary and Westfield College, London, UK<sup>b</sup>*
- <sup>19</sup> *Physics Department, University of Lund, Lund, Sweden<sup>g</sup>*
- <sup>20</sup> *CPPM, CNRS/IN2P3 - Univ. Mediterranee, Marseille - France*
- <sup>21</sup> *Departamento de Física Aplicada, CINVESTAV, Mérida, Yucatán, México<sup>j</sup>*
- <sup>22</sup> *Departamento de Física, CINVESTAV, México<sup>j</sup>*
- <sup>23</sup> *Institute for Theoretical and Experimental Physics, Moscow, Russia<sup>k</sup>*
- <sup>24</sup> *Lebedev Physical Institute, Moscow, Russia<sup>e</sup>*
- <sup>25</sup> *Max-Planck-Institut für Physik, München, Germany*
- <sup>26</sup> *LAL, Université de Paris-Sud 11, IN2P3-CNRS, Orsay, France*
- <sup>27</sup> *LLR, Ecole Polytechnique, IN2P3-CNRS, Palaiseau, France*
- <sup>28</sup> *LPNHE, Universités Paris VI and VII, IN2P3-CNRS, Paris, France*
- <sup>29</sup> *Faculty of Science, University of Montenegro, Podgorica, Montenegro<sup>e</sup>*
- <sup>30</sup> *Institute of Physics, Academy of Sciences of the Czech Republic, Praha, Czech Republic<sup>h</sup>*
- <sup>31</sup> *Faculty of Mathematics and Physics, Charles University, Praha, Czech Republic<sup>h</sup>*
- <sup>32</sup> *Dipartimento di Fisica Università di Roma Tre and INFN Roma 3, Roma, Italy*
- <sup>33</sup> *Institute for Nuclear Research and Nuclear Energy, Sofia, Bulgaria<sup>e</sup>*
- <sup>34</sup> *Institute of Physics and Technology of the Mongolian Academy of Sciences , Ulaanbaatar, Mongolia*
- <sup>35</sup> *Paul Scherrer Institut, Villigen, Switzerland*
- <sup>36</sup> *Fachbereich C, Universität Wuppertal, Wuppertal, Germany*
- <sup>37</sup> *Yerevan Physics Institute, Yerevan, Armenia*
- <sup>38</sup> *DESY, Zeuthen, Germany*
- <sup>39</sup> *Institut für Teilchenphysik, ETH, Zürich, Switzerland<sup>i</sup>*
- <sup>40</sup> *Physik-Institut der Universität Zürich, Zürich, Switzerland<sup>i</sup>*

<sup>41</sup> Also at Physics Department, National Technical University, Zografou Campus, GR-15773 Athens, Greece

<sup>42</sup> Also at Rechenzentrum, Universität Wuppertal, Wuppertal, Germany

<sup>43</sup> Also at University of P.J. Šafárik, Košice, Slovak Republic

<sup>44</sup> Also at CERN, Geneva, Switzerland

<sup>45</sup> Also at Max-Planck-Institut für Physik, München, Germany

<sup>46</sup> Also at Comenius University, Bratislava, Slovak Republic

<sup>47</sup> Also at DESY and University Hamburg, Helmholtz Humboldt Research Award

<sup>48</sup> Supported by a scholarship of the World Laboratory Björn Wiik Research Project

<sup>49</sup> Also at National Institute for Physics and Nuclear Engineering, Magurele, Bucharest, Romania

<sup>a</sup> Supported by the Bundesministerium für Bildung und Forschung, FRG, under contract numbers 05 H1 1GUA /1, 05 H1 1PAA /1, 05 H1 1PAB /9, 05 H1 1PEA /6, 05 H1 1VHA /7 and 05 H1 1VHB /5

<sup>b</sup> Supported by the UK Particle Physics and Astronomy Research Council, and formerly by the UK Science and Engineering Research Council

<sup>c</sup> Supported by FNRS-FWO-Vlaanderen, IISN-IKW and IWT and by Interuniversity Attraction Poles Programme, Belgian Science Policy

<sup>d</sup> Partially Supported by Polish Ministry of Science and Higher Education, grant PBS/DESY/70/2006

<sup>e</sup> Supported by the Deutsche Forschungsgemeinschaft

<sup>f</sup> Supported by VEGA SR grant no. 2/7062/ 27

<sup>g</sup> Supported by the Swedish Natural Science Research Council

<sup>h</sup> Supported by the Ministry of Education of the Czech Republic under the projects LC527 and INGO-1P05LA259

<sup>i</sup> Supported by the Swiss National Science Foundation

<sup>j</sup> Supported by CONACYT, México, grant 400073-F

<sup>k</sup> Partially Supported by Russian Foundation for Basic Research, grants 03-02-17291 and 04-02-16445

<sup>l</sup> This project is co-funded by the European Social Fund (75%) and National Resources (25%) - (EPEAEK II) - PYTHAGORAS II

# 1 Introduction

A search for narrow baryonic states in the mass range 1600 – 2300 MeV, decaying into the doubly charged  $\Xi^- \pi^-$  and neutral  $\Xi^- \pi^+$  final states and their antiparticles<sup>1</sup>, is presented. The search is carried out in deep inelastic  $ep$  scattering (DIS) at HERA.

Various theoretical approaches [1, 2, 3] based on Quantum Chromodynamics predict the existence of exotic baryonic states composed of four valence quarks and an anti-quark, commonly known as “pentaquarks”. Such states are expected to form a flavour anti-decuplet and are not explicitly forbidden within the Standard Model.

Several experiments have reported evidence for a narrow resonance with a mass around 1540 MeV decaying into  $nK^+$  and  $pK_S^0$  final states [4]. Such a state could be interpreted as an exotic strange pentaquark with a minimal quark content of  $uudd\bar{s}$ , lying in the apex of the spin 1/2 (or 3/2) anti-decuplet. On the other hand, a number of other experiments [4], including the H1 experiment [5], have reported non-observation of the same state.

Searches for other members of this anti-decuplet are of interest, in particular for the doubly strange  $\Xi_{5q}^{--}$  ( $ddss\bar{u}$ ) and  $\Xi_{5q}^+$  ( $uuss\bar{d}$ ) states, which are also manifestly exotic. The NA49 collaboration [6] reported the observation of two baryonic resonances in fixed target proton-proton collisions at the SPS at the centre of mass energy  $\sqrt{s} = 17.2$  GeV, with masses of  $1862 \pm 2$  MeV and  $1864 \pm 5$  MeV, and with widths below the mass resolution of 18 MeV. These states can be interpreted as the  $\Xi_{5q}^{--}$  ( $S = -2$ ,  $I_3 = -3/2$ ) and the  $\Xi_{5q}^0$  ( $S = -2$ ,  $I_3 = +1/2$ ) members of the isospin 3/2 quartet  $\Xi_{3/2}$  in the anti-decuplet. These findings have not been confirmed by several other experiments [7, 8, 9, 10, 11, 12].

The search presented here is performed using data taken with the H1 detector at HERA. The  $\Xi^-$  particles are identified through their decay into  $\Lambda\pi^-$ . The established baryon  $\Xi(1530)^0$  [13] is observed through its decay mode  $\Xi(1530)^0 \rightarrow \Xi^- \pi^+$ .

## 2 Experimental Procedure

### 2.1 H1 Apparatus

A detailed description of the H1 detector can be found in [14]. In the following only those detector components important for the present analysis are described.

H1 uses a right handed cartesian coordinate system with the origin at the nominal  $ep$  interaction point. The proton beam direction defines the  $z$  axis. The polar angle  $\theta$  is measured with respect to this axis and the pseudorapidity  $\eta$  is given by  $\eta = -\ln \tan \frac{\theta}{2}$ .

The tracks from charged particles are reconstructed in the central tracker, whose main components are two cylindrical drift chambers, the inner and outer central jet chambers (CJCs) [15], complemented by a central silicon vertex detector (CST) [16]. The CJCs are mounted concentrically around the beam-line, covering the range of pseudorapidity  $-1.75 < \eta < 1.75$  for tracks

---

<sup>1</sup>Unless explicitly mentioned, the charge conjugate states are hereafter always implicitly included.

coming from the nominal interaction point. The CJs lie within a homogeneous magnetic field of 1.16 T which allows the transverse momentum  $p_T$  of charged particles to be measured. Two additional drift chambers (CIZ, COZ) complement the CJs by precisely measuring the  $z$  coordinates of track segments and hence improve the determination of the polar angle. Two cylindrical multi-wire proportional chambers facilitate triggering on tracks. The transverse momentum resolution of the central tracker is  $\sigma(p_T)/p_T \simeq 0.005 p_T / \text{GeV} \oplus 0.015$  [17]. Charge misidentification is negligible for particles originating from the primary vertex and having transverse momenta in the range relevant to this analysis.

The tracking detectors are surrounded by a Liquid Argon calorimeter (LAr) in the forward and central region ( $-1.5 < \eta < 3.4$ ) and by a lead-scintillating fibre calorimeter (SpaCal) in the backward region [18] ( $-4 < \eta < -1.4$ ). The SpaCal is optimised for the detection of the scattered electron<sup>2</sup> in the DIS kinematic range considered here. A planar drift chamber, positioned in front of the SpaCal, improves the measurement of the electron polar angle and is used to reject neutral particle background from photons. The kinematics of the hadronic final state are reconstructed using an algorithm which combines information from the central tracker, the SpaCal and the LAr calorimeter. The DIS events studied in this paper are triggered by an energy deposition in the SpaCal, complemented by signals in the CJs and the multi-wire proportional chambers in the central tracker.

The luminosity is determined from the rate of Bethe-Heitler processes  $ep \rightarrow ep\gamma$ , measured using a calorimeter located close to the beam pipe at  $z = -103$  m in the backward direction.

## 2.2 Selection of DIS Events

The analysis is carried out using data corresponding to an integrated luminosity of  $\mathcal{L} = 101 \text{ pb}^{-1}$ , taken in the years 1996/1997 and 1999/2000. During this time HERA collided electrons or positrons at an energy of 27.6 GeV with protons at 820 GeV (1996/1997,  $24.8 \text{ pb}^{-1}$ ) and 920 GeV (1999/2000,  $75.7 \text{ pb}^{-1}$ ).

The event kinematics are reconstructed from the energy and the polar angle of the scattered electron, which is required to be identified in the SpaCal with an energy above 8 GeV. The negative four momentum transfer squared  $Q^2$  of the exchanged virtual photon and the inelasticity  $y$  are required to lie in the ranges  $2 < Q^2 < 100 \text{ GeV}^2$  and  $0.05 < y < 0.7$ . The difference between the total energy  $E$  and the longitudinal component of the total momentum  $p_z$ , calculated from the electron and the hadronic final state, is restricted to  $35 < E - p_z < 70 \text{ GeV}$ . This requirement suppresses photoproduction background, in which the electron escapes detection and a hadron fakes the electron signature. Events are accepted if the  $z$  coordinate of the event vertex, reconstructed using the central tracker, lies within  $\pm 35$  cm of the mean position for  $ep$  interactions.

## 2.3 Selection of the Baryon Candidates

The hypothetical doubly charged  $X^{--}$  and the neutral  $X^0$  baryon states are identified by complete reconstruction of their respective decay chains through  $\Xi^-$  and  $\Lambda$  baryons into pions and protons, according to

---

<sup>2</sup>Herein, the term ‘‘electron’’ is used generically to refer to both electrons and positrons.

$$X^{--} \rightarrow \Xi^- \pi^- \rightarrow [\Lambda \pi^-] \pi^- \rightarrow [(p \pi^-) \pi^-] \pi^- \quad (1)$$

$$X^0 \rightarrow \Xi^- \pi^+ \rightarrow [\Lambda \pi^-] \pi^+ \rightarrow [(p \pi^-) \pi^-] \pi^+ . \quad (2)$$

The decay daughter particles are fitted in three dimensions to their respective decay vertices [19], which are referred to as the tertiary ( $\Lambda$ -decay) and the secondary ( $\Xi$ -decay) vertex. The analysis is based on charged particles measured in the central region of the H1 detector with a minimal transverse momentum  $p_T$  of 0.12 GeV. These (non vertex-fitted) tracks may in addition be kinematically constrained to the primary vertex, in which case they are specifically referred to as primary vertex-fitted tracks. The baryon selection is chosen to optimise the signal for the standard baryon  $\Xi(1530)^0$ .

In the first step, the  $\Lambda$  baryons are identified by their charged decay mode,  $\Lambda \rightarrow p \pi^-$ , using pairs of oppositely charged tracks. The track with the higher momentum is assigned the proton mass. The particles are fitted to the tertiary vertex and the  $\Lambda$  candidates are retained if the vertex fit probability is above 1%. To reduce background, the two-dimensional separation (in the plane transverse to the beam line) of the tertiary and the primary vertex is required to be larger than 7.5 mm. The transverse momentum of the  $\Lambda$  is required to be larger than 0.3 GeV. The contamination from  $K_S^0 \rightarrow \pi^+ \pi^-$  decays is suppressed by excluding candidates with a  $\pi\pi$  invariant mass in a  $\pm 10$  MeV ( $\sim 2\sigma$ ) window around the nominal  $K_S^0$  mass.  $\Lambda$  candidates are retained for the further steps if their invariant  $p\pi$  mass is within  $\pm 8$  MeV of the nominal  $\Lambda$  mass, which is subsequently assigned to the selected  $\Lambda$  candidates.

In the second step,  $\Xi^-$  candidates are formed by combining each of the  $\Lambda$  candidates with a negatively charged track assumed to be a pion. It is required that: the  $\Lambda$  candidates and the negatively charged tracks be fitted to a secondary vertex with a probability above 0.1 %; the two-dimensional distance of closest approach in the transverse plane ( $DCA$ ) of the  $\Xi^-$  candidates with respect to the primary vertex be smaller than 2.5 mm; the angle between the secondary and the tertiary vertex vectors<sup>3</sup> be less than 0.6 rad. The invariant mass spectra  $M(\Lambda\pi^-)$  and  $M(\bar{\Lambda}\pi^+)$  of all candidates passing these criteria are shown in figure 1. Clear signal peaks are observed around the nominal  $\Xi^-$  mass.  $\Xi^-$  candidates are retained for the third step if their invariant mass is within  $\pm 15$  MeV of the nominal  $\Xi^-$  mass, which is subsequently assigned to the selected  $\Xi^-$  candidates.

In the third step,  $X^{--/0}$  baryon candidates are formed by combining each  $\Xi^-$  candidate with one additional primary vertex-fitted track assumed to be a pion. For these combinations it is required that: the additional  $\pi^\pm$  track have a significance ( $DCA/\sigma_{DCA}$ ) to the primary vertex of less than 4.0; the transverse momentum of the  $X^{--/0}$  candidates be larger than 1.0 GeV and their pseudorapidity be within  $|\eta| < 1.5$ .

## 2.4 Simulation of Baryonic States

To estimate the acceptance, the efficiency and the resolution for the detection of a hypothetical baryon state, a Monte Carlo simulation based on the PYTHIA [20] event generator is used,

---

<sup>3</sup>A vertex vector is defined as the vector pointing from the primary vertex to the given vertex.

incorporating the Lund string model of fragmentation [21]. The kinematic distributions of strange  $S = -1$  hadrons in DIS data have been found to be reasonably well described [22] by the PYTHIA simulation. A generic  $X^{--}$  baryon state is introduced in the simulation by changing the mass of the known  $\bar{\Delta}^{--}$  antibaryon to values in the required range from 1600 – 2300 MeV and having it decay into  $\Xi^- \pi^-$  final states. Because most theoretical predictions and the measurements [4] suggest a very small intrinsic width  $\sigma \lesssim 1$  MeV for pentaquark states, the width for the  $X^{--}$  is assumed to be zero in the simulation. Due to lack of knowledge of the pentaquark production mechanism, it is assumed that the production kinematics of the  $X^{--}$  are similar to those of the standard  $\Xi(1530)^0$  baryon. The generic  $X^0$  state is introduced by changing the mass of the known  $\Xi(1530)^0$  baryon to values in the required range from 1600 – 2300 MeV, and letting it decay into  $\Xi^- \pi^+$ . All the generated events are passed through a detailed simulation of the H1 detector response based on the GEANT program [23] and the same reconstruction and analysis algorithms as used for the data.

### 3 Mass Spectra and Limit Calculation

The resulting invariant mass spectra for each of the two neutral ( $\Xi^- \pi^+$ ,  $\bar{\Xi}^+ \pi^-$ ) and the two doubly charged combinations ( $\Xi^- \pi^-$ ,  $\bar{\Xi}^+ \pi^+$ ) are shown separately in figure 2. In both neutral spectra the signal of the well known  $\Xi(1530)^0$  state is observed. The sum of the two neutral and of the two doubly charged mass spectra are shown in the upper part of figures 3 and 4, respectively.

The ratio of the invariant mass spectra of the neutral to the charged states is consistent with being flat in the mass region above the  $\Xi(1530)^0$  mass. This justifies the use of the same background shape function for both the doubly charged and the neutral combinations. A simultaneous fit of the neutral and the doubly charged mass spectra, shown in figures 3 and 4, is performed using a function  $F$ , that contains a Gaussian function  $G$  for the signal  $\Xi(1530)^0$  baryon and a function  $B$  for the background shape, according to

$$F = G + (1 + P_0)B; \quad B(M) = P_1(M - m_\Xi - m_\pi)^{P_2} \times (1 + P_3M + P_4M^2). \quad (3)$$

Here,  $M$  denotes the  $\Xi\pi$  invariant mass and  $m_\Xi$  and  $m_\pi$  the masses of the  $\Xi$  and the  $\pi$ , respectively. The normalisation, the central value and the width of the Gaussian function  $G$  and the parameters  $P_i$  are left free in the fit.  $P_0$  represents the relative normalisation of the neutral to the doubly charged combinations and is set to zero for the neutral combinations. The fit yields a total of  $163 \pm 24$  (*stat.*)  $\Xi(1530)^0$  baryons. The reconstructed mass of  $1532 \pm 2$  (*stat.*) MeV is consistent with the nominal value [13]. The measured width of  $9.4 \pm 1.5$  (*stat.*) MeV is in agreement with the detector simulation.

No signal of a new baryonic state is observed above the  $\Xi(1530)^0$  mass in either the neutral or the doubly charged mass spectra (figures 3 and 4). The resonance search can also be performed relative to the observed signal of the known  $\Xi(1530)^0$  baryon, using the ratio  $R$ , which is defined as

$$R(M) = \frac{N^{res}(M, q)}{N(1530, 0)} \times \frac{\epsilon(1530, 0)}{\epsilon(M, q)}. \quad (4)$$

$N(1530, 0)$  represents the number of observed  $\Xi(1530)^0 \rightarrow \Xi^- \pi^+$  and their antiparticle decays.  $N^{res}(M, q)$  describes the estimated number of resonance decays depending on the mass  $M$  and the charge  $q$  of the final state, which is derived from the difference between the observed spectra and the expected background contribution. The background distribution is taken to be the fitted function given by equation 3. For the calculation of  $N^{res}$ , the mass distribution of the signal is assumed to be a Gaussian function with a mean  $M$  and a mass-dependent width  $\sigma(M)$  corresponding to the experimental mass resolution. This width  $\sigma(M)$  varies from 6.8 to 22.8 MeV in the mass range considered here, as obtained from the Monte Carlo simulation. The term  $\epsilon(M, q)$  describes the reconstruction efficiency of the  $\Xi \pi$  final state as determined by Monte Carlo simulation, and it depends on the  $\Xi \pi$  invariant mass  $M$  and on the charge  $q$  of the final state. Accordingly,  $\epsilon(1530, 0)$  represents the reconstruction efficiency for the neutral  $\Xi(1530)^0$  baryon. The ratio of efficiencies in equation 4 compensates for the small difference in the reconstruction efficiencies of the  $\Xi(1530)^0$  baryon and of a hypothetical baryon state. This factor varies from 0.96 (0.92) at the smallest masses to 0.87 (0.86) at the highest masses considered for the neutral (doubly charged) states.

The ratio  $R(M)$  has the advantage that the systematic effects of the acceptances and the reconstruction efficiencies mostly cancel, making it insensitive to detector effects. In the absence of an observed signal, the ratio  $R(M)$  therefore provides a robust quantity to set upper limits on the production of new narrow baryonic resonances decaying to  $\Xi^- \pi^\pm$  in the mass range 1600 – 2300 MeV. A mass-dependent upper limit at the 95% confidence level (C.L.) on the ratio  $R(M)$  is obtained from the observed invariant mass spectra using a modified frequentist approach based on likelihood ratios [24] analogous to the one applied in [5]. The method takes the statistical and systematic uncertainties in the number of signal events and background combinations into account.

The systematic uncertainties on the ratio  $R(M)$  include the following contributions:

1. The uncertainty on the overall number of  $\Xi(1530)^0$  candidates is 15%, as determined from the fit to the mass spectra.
2. The statistical uncertainty on the determination of the reconstruction efficiency  $\epsilon(M, q)$  by the Monte Carlo simulation is taken as the value of the systematic uncertainty on the ratio  $\epsilon(1530, 0)/\epsilon(M, q)$ . It is found to be below 8% for all masses and charge combinations considered. Systematic uncertainties due to the lack of knowledge of the production mechanism of the hypothetical new baryon state are not taken into account.
3. An uncertainty on the experimental width of the potential pentaquark signal is estimated to be 5%, as determined by the difference of the observed width of the  $\Xi(1530)^0$  signal in data and simulation.
4. A systematic uncertainty on the background distribution is assessed by performing the fit under different assumptions: using the background function (3) in the full mass range, excluding a mass window of  $\pm 2\sigma$  around the considered mass, and also using the sum

of the background function and a Gaussian with fixed mass  $M$  and width  $\sigma(M)$  to account for a possible signal. The uncertainty of the number of background combinations is estimated from the difference between the different fitting methods and amounts to 2%.

In the limit calculation, the contributions from items 1-3 are quadratically added and included in the uncertainty on the signal events, while the contribution from item 4 enters the background uncertainty.

The final results of the limit calculations are quoted for the kinematic region  $2 < Q^2 < 100 \text{ GeV}^2$  and  $0.05 < y < 0.7$ , for  $p_T(\Xi\pi) > 1 \text{ GeV}$  and  $|\eta(\Xi\pi)| < 1.5$ . As stated before, it is assumed that new resonances are produced by a similar mechanism to that of the known  $J = 3/2$  baryons, that they decay into  $\Xi\pi$  with a 100% branching ratio, and that their natural widths are below the experimental resolution.

In figure 3 the  $\Xi^-\pi^-$  invariant mass spectrum summed over the two doubly charged combinations is shown. In the same figure the 95% C.L. upper limit on the ratio  $R(M)$  is presented as a function of the mass  $M$ . The non-observation of a resonance state in the mass range 1600 – 2300 MeV limits the production rate of a hypothetical  $\Xi_{5q}^{--}$  pentaquark to 12 – 45% of the  $\Xi(1530)^0$  production rate at the 95% C.L., depending on the  $(\Xi\pi)$ -mass.

Furthermore, no signal is observed in the neutral invariant mass spectrum (figure 4) in the mass range 1600 – 2300 MeV, above the  $\Xi(1530)^0$  baryon. Figure 4 also shows the resulting upper limit on the ratio  $R(M)$ , which is obtained in a procedure analogous to the doubly charged case. This restricts the production rate of a hypothetical  $\Xi_{5q}^0$  pentaquark state to less than 10 – 50% of that of the  $\Xi(1530)^0$  baryon, depending on the  $(\Xi\pi)$ -mass.

This result is similar to the 10 – 50% upper limits measured by the ZEUS Collaboration [12] in the region  $Q^2 > 1 \text{ GeV}^2$ .

## 4 Conclusion

A search for new narrow baryonic resonances decaying into  $\Xi^-\pi^-$  and  $\Xi^-\pi^+$  and their charge conjugate states is performed with the H1 detector using a DIS data sample in the kinematic region  $2 < Q^2 < 100 \text{ GeV}^2$  and  $0.05 < y < 0.7$ , corresponding to a total integrated luminosity of  $101 \text{ pb}^{-1}$ . The established  $\Xi(1530)^0$  baryon state is observed. No signal of a new baryonic state is found in the mass range 1600 – 2300 MeV. Therefore mass dependent upper limits at the 95% C.L. are set on the production ratio of hypothetical states, such as  $\Xi_{5q}^{--}$  and  $\Xi_{5q}^0$ , to the total number of observed  $\Xi(1530)^0$  baryons.

The results reported here are similar to the limits measured by the ZEUS Collaboration. The overall H1 statistics in the  $\Xi^-$  samples is comparable with the NA49 collaboration's data. The H1 limits obtained at HERA do not confirm the NA49 observation of potential pentaquark states.

## Acknowledgements

We are grateful to the HERA machine group whose outstanding efforts have made this experiment possible. We thank the engineers and technicians for their work in constructing and maintaining the H1 detector, our funding agencies for financial support, the DESY technical staff for continual assistance and the DESY directorate for support and for the hospitality which they extend to the non DESY members of the collaboration.

## References

- [1] D. Diakonov, V. Petrov and M. V. Polyakov, *Z. Phys. A* **359** (1997) 305 [hep-ph/9703373].
- [2] R. L. Jaffe and F. Wilczek, *Phys. Rev. Lett.* **91** (2003) 232003 [hep-ph/0307341];  
for a review on pentaquark phenomenology see R. L. Jaffe, *Phys. Rept.* **409** (2005) 1,  
[hep-ph/0409065].
- [3] M. Karliner and H. J. Lipkin, *Phys. Lett. B* **575** (2003) 249 [hep-ph/0402260,hep-ph/0307243].
- [4] For a review on the experimental search for pentaquark states, see  
K. H. Hicks, *Prog. Part. Nucl. Phys.* **55** (2005) 647 [hep-ex/0504027].
- [5] A. Aktas *et al.* [H1 Collaboration], *Phys. Lett. B* **639** (2006) 202 [hep-ex/0604056].
- [6] C. Alt *et al.* [NA49 Collaboration], *Phys. Rev. Lett.* **92** (2004) 042003 [hep-ex/0310014].
- [7] M. I. Adamovich *et al.* [WA89 Collaboration], *Phys. Rev. C* **70** (2004) 022201 [hep-ex/0405042].
- [8] S. Schael *et al.* [ALEPH Collaboration], *Phys. Lett. B* **599** (2004) 1.
- [9] J. Z. Bai *et al.* [BES Collaboration], *Phys. Rev. D* **70** (2004) 012004 [hep-ex/0402012].
- [10] I. Abt *et al.* [HERA-B Collaboration], *Phys. Rev. Lett.* **93** (2004) 212003 [hep-ex/0408048].
- [11] A. Airapetian *et al.* [HERMES Collaboration], *Phys. Rev. D* **71** (2005) 032004 [hep-ex/0412027].
- [12] S. Chekanov *et al.* [ZEUS Collaboration], *Phys. Lett. B* **610** (2005) 212 [hep-ex/0501069].
- [13] W. M. Yao *et al.* [Particle Data Group], *J. Phys. G* **33**, 1 (2006).
- [14] I. Abt *et al.* [H1 Collaboration], *Nucl. Inst. Meth. A* **386** (1997) 310;  
I. Abt *et al.* [H1 Collaboration], *Nucl. Inst. Meth. A* **386** (1997) 348.
- [15] J. Bürger *et al.*, *Nucl. Instrum. Meth. A* **279** (1989) 217.
- [16] D. Pitzl *et al.*, *Nucl. Instrum. Meth. A* **454** (2000) 334 [hep-ex/0002044].

- [17] C. Kleinwort, Contribution to “LHC Tracking and Alignment Workshop”, CERN, Sep. 2006.
- [18] R. D. Appuhn *et al.* [H1 SpaCal Group], Nucl. Inst. Meth. A **386** (1997) 397.
- [19] R. Luchsinger and C. Grab, Comput. Phys. Commun. **76** (1993) 263.
- [20] T. Sjöstrand *et al.*, Pythia 6.2, Comput. Phys. Commun. **135** (2001) 238 [hep-ph/0010017].
- [21] B. Andersson, G. Gustafson, G. Ingelman and T. Sjöstrand, Phys. Rept. **97** (1983) 31.
- [22] M. Derrick *et al.* [ZEUS Collaboration], Z. Phys. C **68** (1995) 29 [hep-ex/9505011]; S. Aid *et al.* [H1 Collaboration], Nucl. Phys. B **480**, (1996) 3 [hep-ex/9607010];  
C. Risler, Ph.D. thesis, 2004, Universität Hamburg (in German), available from <http://www-h1.desy.de/publications/theses.list.html>;  
S. Chekanov *et al.* [ZEUS Collaboration], [hep-ex/0612023].
- [23] R. Brun *et al.*, GEANT3, Technical Report CERN-DD/EE/84-1, CERN, 1987.
- [24] T. Junk, Nucl. Instrum. Meth. A **434** (1999) 435 [hep-ex/9902006].

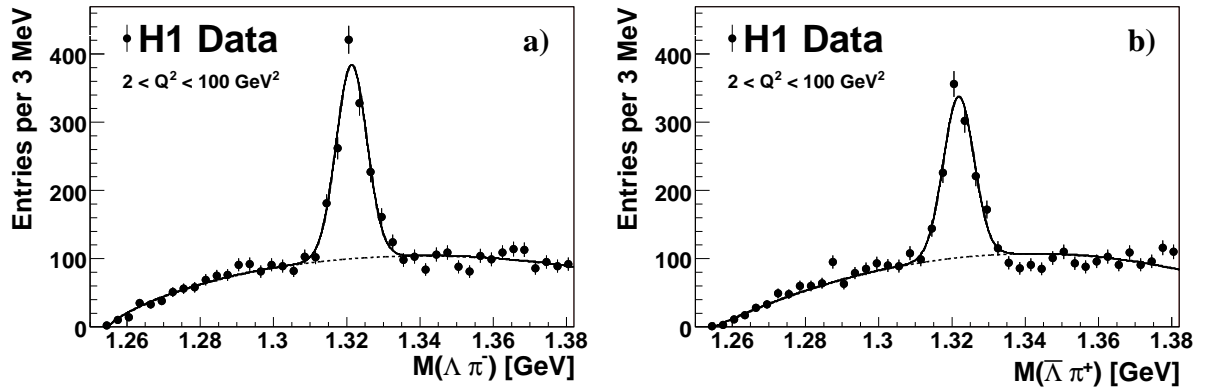


Figure 1: The invariant mass spectra for a)  $\Lambda\pi^-$  and b)  $\bar{\Lambda}\pi^+$  particle combinations. The solid lines show the result of a fit to the data using a Gaussian function for the  $\Xi^-$  signal and a background function as defined in equation 3 (with  $m_{\Xi}$  replaced accordingly by  $m_{\Lambda}$ ), while the dashed lines indicate the background function only.

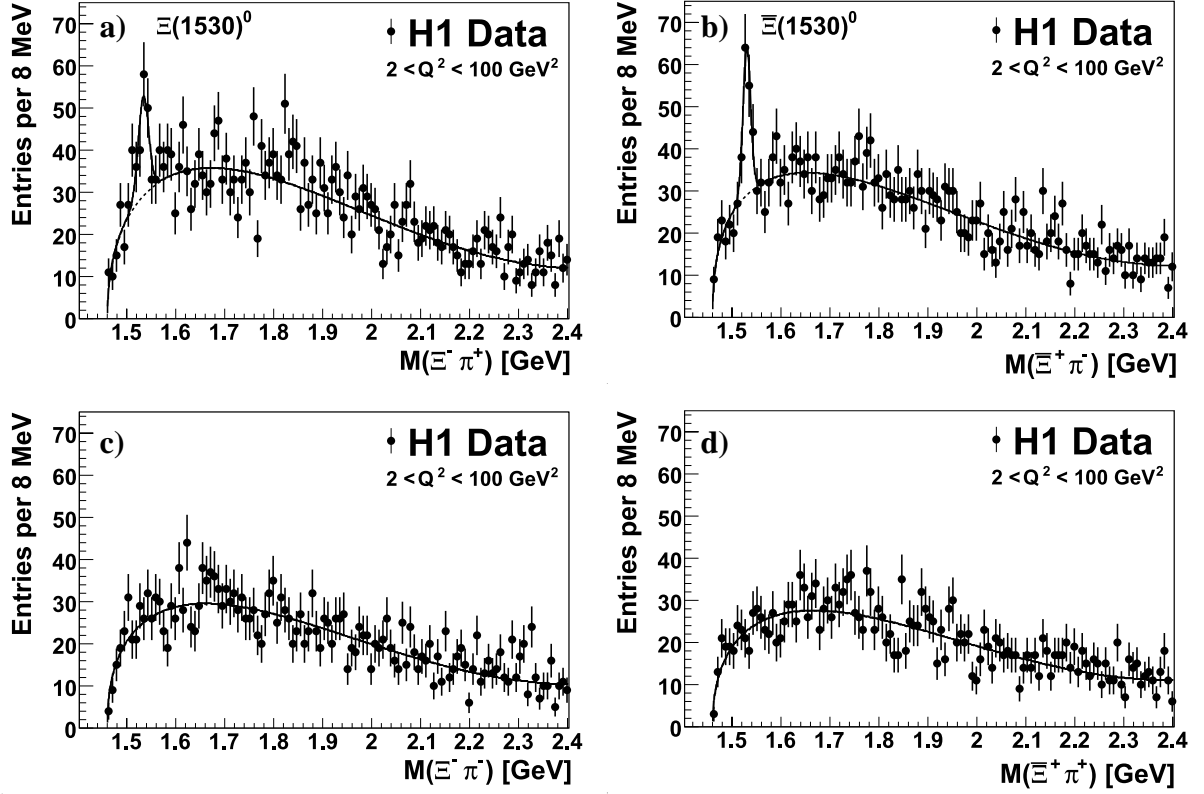


Figure 2: The invariant mass spectra of the  $\Xi\pi$  particle combinations for the charge combinations a)  $\Xi^-\pi^+$ , b)  $\Xi^+\pi^-$ , c)  $\Xi^-\pi^-$  and d)  $\Xi^+\pi^+$ . For the purpose of illustration, the solid lines in a) and b) show the result of a fit to the data using a Gaussian function for the  $\Xi(1530)^0$  signal and a background function (dashed lines) as defined in equation 3. The same background parametrisation is used in c) and d).

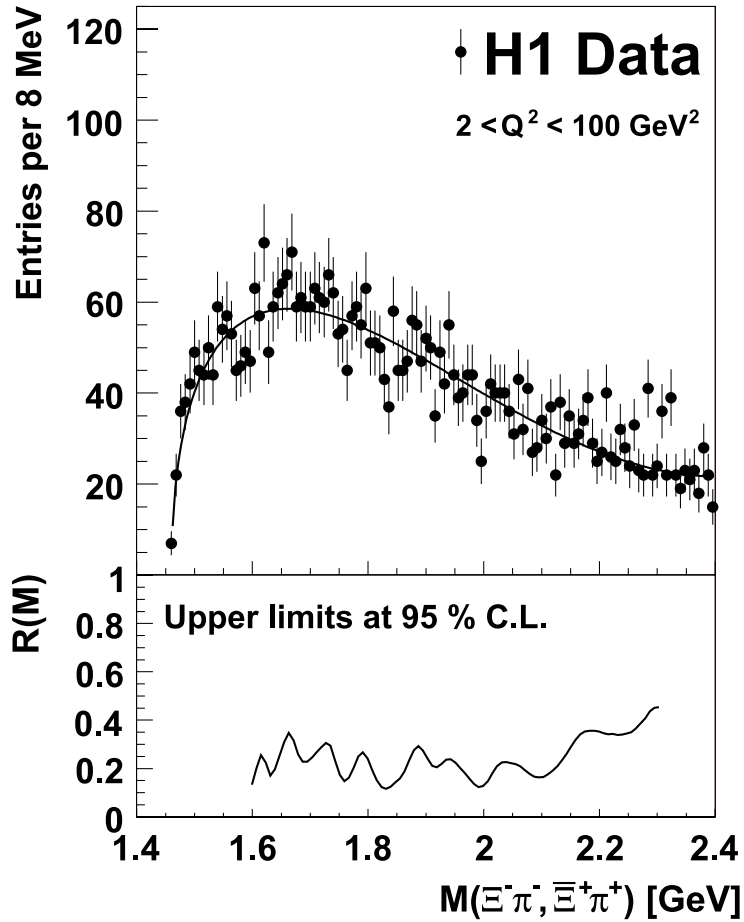


Figure 3: The invariant mass spectrum for the doubly charged combinations  $\Xi^-\pi^-$  and  $\Xi^+\pi^+$  (upper part). The solid line shows the result of a fit to the data using a background function as defined in equation 3. The lower part shows the 95% C.L. upper limit on the ratio  $R(M)$  as a function of the mass  $M$ , as defined in equation 4.

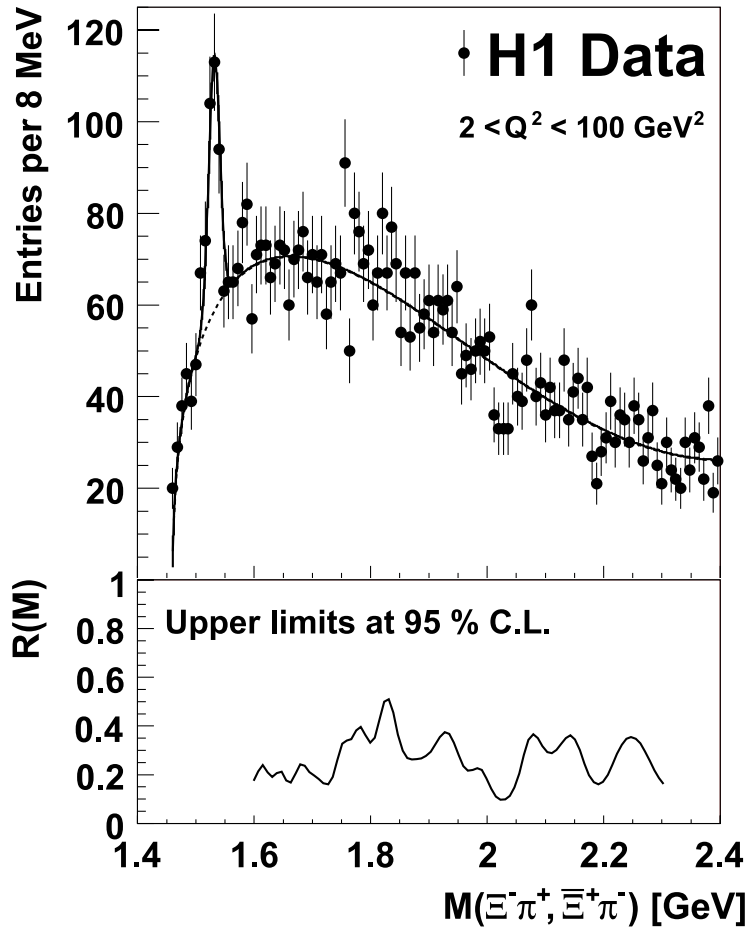


Figure 4: The invariant mass spectrum for the neutral combinations  $\Xi^- \pi^+$  and  $\Xi^+ \pi^-$  (upper part). The solid line shows the result of a fit to the data using a Gaussian function for the  $\Xi(1530)^0$  signal and a background function (dashed line) as defined in equation 3. The lower part shows the 95% C.L. upper limit on the ratio  $R(M)$  as a function of the mass  $M$ , as defined in equation 4.